
(This is a sample cover image for this issue. The actual cover is not yet available at this time.)

Journal of Non-Newtonian Fluid Mechanics 171-172 (2012) 83–96

Contents lists available at SciVerse ScienceDirect

Journal of Non-Newtonian Fluid Mechanics

journal homepage: http://www.elsevier.com/locate/jnnfm

# Laminar Rayleigh-Bénard convection of yield stress fluids in a square enclosure

Osman Turan [a,b], Nilanjan Chakraborty [c], Robert J. Poole [a,*]

[a] School of Engineering, University of Liverpool, Brownlow Hill, Liverpool L69 3GH, UK
[b] Department of Mechanical Engineering, Karadeniz Technical University, Trabzon 61080, Turkey
[c] School of Mechanical and Systems Engineering, Newcastle University, Claremont Road, Newcastle-Upon-Tyne NE1 7RU, UK

ARTICLE INFO

*Article history:*
Received 30 November 2011
Received in revised form 16 January 2012
Accepted 17 January 2012
Available online 1 February 2012

*Keywords:*
Rayleigh-Bénard configuration
Natural convection
Rayleigh number
Prandtl number
Grashof number
Bingham number

ABSTRACT

In this study, two-dimensional steady-state simulations of laminar natural convection in square enclosures with differentially heated horizontal walls with the bottom wall at higher temperature have been conducted for yield-stress fluids obeying the Bingham model. Heat and momentum transport are investigated for nominal values of Rayleigh number ($Ra$) in the range $10^3$–$10^5$ and a Prandtl number ($Pr$) range of 0.1–100. The mean Nusselt number $\overline{Nu}$ is found to increase with increasing values of Rayleigh number for both Newtonian and Bingham fluids. However, weaker convective transport in Bingham fluids leads to smaller values of $\overline{Nu}$ than that obtained in the case of Newtonian fluids with the same nominal value of Rayleigh number $Ra$. The mean Nusselt number $\overline{Nu}$ decreases with increasing Bingham number in the case of yield stress fluids, and, for large values of Bingham number $Bn$, the value rapidly approaches to unity ($\overline{Nu} = 1.0$) as thermal conduction dominates the heat transfer. However, this variation in the present configuration is found to be markedly different from the corresponding variation of $\overline{Nu}$ with $Bn$ for the same nominal values of $Ra$ and $Pr$ in the differentially-heated vertical sidewall configuration. The effects of Prandtl number have also been investigated in detail and physical explanations are provided for the observed behaviour. Guided by a detailed scaling analysis, new correlations are proposed for the mean Nusselt number $\overline{Nu}$ for both Newtonian and Bingham fluids which are demonstrated to satisfactorily capture the correct qualitative and quantitative behaviours of $\overline{Nu}$ for the range of $Ra$, $Pr$ and $Bn$ considered in this analysis.



## 1. Introduction

Natural convection of fluid contained in rectangular enclosures is one of the most widely studied configurations in thermal fluids problems due, in part, to its relevance in solar collectors, electronic cooling, energy storage and management and food preservation and heating. In addition to these applications it is a prototypical geometry which allows many fundamental issues to be studied in a well-controlled way. Ostrach [1] provides an extensive review of such flows. Different configurations for natural convection in rectangular enclosures are possible depending on the exact boundary conditions at the enclosure walls. One of the most important configurations is where the horizontal walls are differentially heated with the bottom wall kept at higher temperature and the vertical walls insulated, which is referred to as the Rayleigh-Bénard configuration in the present analysis. It is worth highlighting here that the *classical* Rayleigh-Bénard configuration is considered to be long and wide in the horizontal direction to avoid the influences of vertical walls [2,3]. However, natural convection in finite-sized enclosures with differentially-heated horizontal walls with the bottom wall at higher temperature is often loosely referred to as "Rayleigh-Bénard" in the heat transfer literature (see Refs. [4–8]) and we choose to adopt this convention in the current manuscript for the sake of a concise description of the boundary condition in the subsequent discussion. The analysis presented in this paper focuses on the Rayleigh-Bénard (RB) configuration and thus the discussion in the remainder of this introduction, unless otherwise stated, will be confined to this particular boundary condition.

To date, most numerical studies of RB natural convection in rectangular enclosures have been carried out for Newtonian fluids (Refs. [1,4,6,8] and references therein provides a detailed overview of this literature) and comparatively limited effort has been expended on the study of RB natural convection of non-Newtonian fluids in rectangular enclosures. Here the natural convection of so-called yield stress materials in RB configuration has been considered (inelastic shear-thinning fluids have been investigated in Refs. [9,10] and viscoelastic fluids in Refs. [5,7]). Yield stress materials behave like a solid material below some critical (yield) stress but are fluid-like beyond this stress. In particular, this analysis primarily concentrates on the fluid flow effects on the heat-transfer characteristics i.e. once the material has yielded. Although a number of studies have probed the effects of yield stress on the hydrodynamic

* Corresponding author. Tel.: +44 1517944806; fax: +44 1517944848.
*E-mail addresses:* osmanturan@ktu.edu.tr (O. Turan), nilanjan.chakraborty@ncl.ac.uk (N. Chakraborty), robpoole@liv.ac.uk (R.J. Poole).

0377-0257/$ - see front matter © 2012 Elsevier B.V. All rights reserved.
doi:10.1016/j.jnnfm.2012.01.006

**Nomenclature**

| | |
|---|---|
| $B$ | Oldroyd number (–) |
| $Bn$ | Bingham number (–) |
| $c_p$ | specific heat at constant pressure (J/kg K) |
| $e$ | relative error (–) |
| $F_s$ | factor of safety (–) |
| $g$ | gravitational acceleration (m/s$^2$) |
| $h$ | heat transfer coefficient (W/m$^2$ K) |
| $k$ | thermal conductivity (W/mK) |
| $L$ | length and height of the enclosure (m) |
| $Pr$ | Prandtl number (–) |
| $q$ | heat flux (W/m$^2$) |
| $Ra$ | Rayleigh number (–) |
| $T$ | temperature (K) |
| $u_i$ | $i$th velocity component (m/s) |
| $U$, $V$ | dimensionless horizontal ($U = u_1 L/\alpha$) and vertical velocity ($V = u_2 L/\alpha$) (–) |
| $\vartheta$ | characteristic velocity (m/s) |
| $x_i$ | coordinate in $i$th direction (m) |
| $\alpha$ | thermal diffusivity (m$^2$/s) |
| $\beta$ | coefficient of thermal expansion (1/K) |
| $\delta$, $\delta_{th}$ | velocity and thermal boundary layer thickness (m) |
| $\theta$ | dimensionless temperature ($\theta = (T - T_C)/(T_H - T_C)$) (–) |
| $\mu$ | plastic viscosity (Ns/m$^2$) |
| $\mu_{yield}$ | yield viscosity (Ns/m$^2$) |
| $\rho$ | density (kg/m$^3$) |
| $\tau_y$ | yield stress (N/m$^2$) |
| $\varphi$ | general primitive variable |
| $\Psi$ | stream function (m$^2$/s) |

*Subscripts*

| | |
|---|---|
| $cv$ | control volume |
| $C$ | cold wall |
| $ext$ | extrapolated value |
| $eff$ | effective value |
| $H$ | hot wall |
| max | maximum value |
| $ref$ | reference value |
| $wall$ | wall value |

*Superscript*

| | |
|---|---|
| cond | value according to pure conduction solution |

*Special characters*

| | |
|---|---|
| $\Delta T$ | difference between hot and cold wall temperature ($=(T_H - T_C)$) (K) |
| $\Delta_{\min,cell}$ | minimum cell distance (m) |
| $r$ | grid expansion ratio (–) |

stability of RB natural convection [2], and investigated weakly nonlinear convection [11], the effects of yield stress for $Ra$ well above the critical conditions have hitherto not been investigated. The aim of this paper is therefore to investigate the effects of yield stress, Rayleigh and Prandtl numbers on the mean Nusselt number in the Rayleigh-Bénard configuration using two regularizations of the well-known Bingham model. The Bingham model is the simplest model for yield stress fluids, as it assumes a linear strain rate dependence of shear stress for the yielded fluid (i.e. beyond the yield stress). Recently, Vola et al. [12] and Turan et al. [13–15] have used the Bingham model to numerically investigate the related problem of natural convection and heat transfer characteristics of yield stress fluids in rectangular enclosures with differentially-heated vertical sidewalls. However, convection initiates as soon as a temperature difference is induced in the differentially heated vertical sidewall configuration, whereas convection starts only when a critical Rayleigh number is surpassed in the RB configuration. Thus the behaviour of $\overline{Nu}$ in response to the weakening of convection due to increasing yield stress in Bingham fluids in the RB configuration is expected to be qualitatively and quantitatively different from the differentially-heated vertical sidewall configuration with the same nominal values of Rayleigh and Prandtl numbers.

In the present study the effects of yield stress on heat and momentum transport for a square enclosure in the Rayleigh-Bénard configuration has been analysed for a large range of Rayleigh numbers ($10^3 < Ra < 10^5$) and Prandtl numbers ($0.1 < Pr < 100$). The wide range of Prandtl numbers considered in this study enables the development of a robust correlation for the mean Nusselt number. Although real yield stress fluids are unlikely to have such low $Pr$ values, such as $Pr = 0.1$, which is characteristic of molten metals, they are included here for the sake of completeness.

## 2. Models for yield stress and non-dimensional groups

The Bingham model for yield stress fluids can be expressed in the following manner [16]:

$$\underline{\underline{\dot{\gamma}}} = 0 \quad \text{for} \quad \tau \leqslant \tau_y, \tag{1}$$

$$\underline{\underline{\tau}} = \left(\mu + \frac{\tau_y}{\dot{\gamma}}\right)\underline{\underline{\dot{\gamma}}} \quad \text{for} \quad \tau > \tau_y, \tag{2}$$

where $\dot{\gamma}_{ij} = \partial u_i/\partial x_j + \partial u_j/\partial x_i$ are the components of the rate of strain tensor $\underline{\underline{\dot{\gamma}}}$, $\underline{\underline{\tau}}$ is the stress tensor, $\tau_y$ is the yield stress, $\mu$ is the so-called plastic viscosity of the yielded fluid, $\tau$ and $\dot{\gamma}$ are the second invariants of the stress and the rate of strain tensors in a pure shear flow respectively, which are expressed as:

$$\tau = \left[\frac{1}{2}\underline{\underline{\tau}} : \underline{\underline{\tau}}\right]^{1/2}, \tag{3}$$

$$\dot{\gamma} = \left[\frac{1}{2}\underline{\underline{\dot{\gamma}}} : \underline{\underline{\dot{\gamma}}}\right]^{1/2}. \tag{4}$$

O'Donovan and Tanner [17] proposed the bi-viscosity model to mimic the stress-shear rate characteristics for a Bingham fluid as:

$$\underline{\underline{\tau}} = \mu_{yield}\underline{\underline{\dot{\gamma}}} \quad \text{for} \quad \dot{\gamma} \leqslant \frac{\tau_y}{\mu_{yield}}, \tag{5}$$

$$\underline{\underline{\tau}} = \left[\frac{\tau_y}{\dot{\gamma}} - \frac{\mu}{\mu_{yield}}\frac{\tau_y}{\dot{\gamma}}\right]\underline{\underline{\dot{\gamma}}} + \mu\underline{\underline{\dot{\gamma}}} \quad \text{for} \quad \dot{\gamma} > \frac{\tau_y}{\mu_{yield}}, \tag{6}$$

where $\mu_{yield}$ is yield viscosity, and $\mu$ the plastic viscosity. This model replaces the solid material by a fluid of high viscosity and it was suggested by O'Donovan and Tanner [17] that a value of $\mu_{yield}$ equal to 1000 $\mu$ mimics the true Bingham model in a satisfactory manner (with the proviso, of course, that below the yield stress the material still flows albeit very slowly). In the present study the bi-viscosity model is predominantly used but in order to assess the sensitivity of the simulations to the regularisation, a limited number of simulations have also been carried out based on the regularisation proposed by Papanastasiou [18]:

$$\underline{\underline{\tau}} = \left[\frac{\tau_y}{\dot{\gamma}}(1 - e^{-m\dot{\gamma}}) + \mu\right]\underline{\underline{\dot{\gamma}}}, \tag{7}$$

where $m$ is the stress growth exponent which has the dimension of time. The regularisation given by Eq. (7) also transforms the "unyielded" region to a zone of high viscosity but removes the

discontinuity inherent in the bi-viscosity approach. Previous studies [13–15] have shown that the maximum difference between the mean Nusselt numbers predicted by the bi-viscosity and Papanastasiou regularisations for a given set of values of nominal Rayleigh, Prandtl and Bingham numbers remains of the order of typical experimental and numerical uncertainties (~2–3%).

In the present study, the heat transfer rate characteristics of Bingham fluids in a square enclosure (of dimension $L$) is compared with the heat transfer rate obtained in the case of Newtonian fluid flows with the same nominal Rayleigh number $Ra$. The Rayleigh number $Ra$ denotes the ratio of the strengths of thermal transport due to buoyancy force to that due to thermal conduction, which is defined in the present study in the following manner:

$$Ra = \frac{\rho^2 c_p g \beta \Delta T L^3}{\mu . k} = GrPr, \tag{8}$$

where $Gr$ is the Grashof number and $Pr$ is the Prandtl number, which are defined as:

$$Gr = \frac{\rho^2 g \beta \Delta T L^3}{\mu^2} \quad \text{and} \quad Pr = \frac{\mu c_p}{k}. \tag{9}$$

The Grashof number provides the ratio of the strengths of buoyancy and viscous forces while the Prandtl number depicts the ratio of momentum diffusion to thermal diffusion. Alternatively, the Prandtl number can be taken to represent the ratios of viscous boundary layer to thermal boundary-layer thicknesses. These definitions are referred to as "nominal" values as they contain the constant plastic viscosity $\mu$. Using Buckingham's pi theorem it is possible to show that for natural convection of Bingham fluids in a square enclosure: $Nu = f_1(Ra, Pr, Bn)$ where the Nusselt number $Nu$ and Bingham number $Bn$ are given by:

$$Nu = \frac{h \cdot L}{k} \quad \text{and} \quad Bn = \frac{\tau_y}{\mu}\sqrt{\frac{L}{g\beta\Delta T}}, \tag{10}$$

where $Nu$ represents the ratio of heat transfer rate by convection to that by conduction in the fluid in question and the heat transfer coefficient $h$ is defined as:

$$h = \left| -k \frac{\partial T}{\partial x_2}\bigg|_{wf} \times \frac{1}{(T_{wall} - T_{ref})} \right|, \tag{11}$$

where subscript 'wf' refers to the condition of the fluid in contact with the wall, $T_{wall}$ is the wall temperature and $T_{ref}$ is the appropriate reference temperature, which can be taken to be $T_C$ ($T_H$) for the hot (cold) wall respectively. The Bingham number $Bn$ represents the ratio of yield stress to viscous stresses. In Eq. (10) the viscous stress ($= \mu\sqrt{g\beta\Delta TL}/L$) is estimated based on velocity and length scales given by $\sqrt{g\beta\Delta TL}$ and $L$ respectively. In Bingham fluid flows the viscosity varies throughout the flow and an effective viscosity expressed as: $\mu_{eff} = \tau_y/\dot{\gamma} + \mu$ might be more representative of the viscous stress within the flow than the constant plastic viscosity $\mu$. Therefore the Rayleigh, Prandtl and Bingham numbers could have been defined more appropriately if $\mu_{eff}$ was used instead of $\mu$. However $\dot{\gamma}$ is expected to show local variations in the flow domain so using a single characteristic value in the definitions of the non-dimensional numbers may not yield any additional benefit in comparison to the definitions given by Eqs. (8)–(10). It is also worth noting that $Bn$ is not the same as the Bingham number "$B$" defined in Ref. [2] and elsewhere – which perhaps should be called an Oldroyd number. The Oldroyd number of Ref. [2] represents the ratio of yield force to buoyancy force and is related to $Bn$ used here through the following expression: $B = Bn/Gr^{1/2} = Bn\sqrt{Pr/Ra}$.

In the present study the effects of $Ra$, $Bn$ and $Pr$ on $Nu$ are investigated systematically and suitable correlations proposed. However, it is worth noting that in the present study the plastic viscosity $\mu$ and yield stress $\tau_y$ are taken to be independent of temperature both for the sake of simplicity and also due to the experimental evidence that the yield stress remains approximately independent of temperature and the plastic viscosity is only a weakly decreasing function of temperature for a well-known yield stress system ("Carbopol") in the temperature range 0–90 °C [19].

## 3. Numerical method

A finite-volume code is used to solve the coupled conservation equations of mass, momentum and energy. In this framework, a second-order central differencing is used for the diffusive terms and a second-order up-wind scheme for the convective terms. Coupling of the pressure and velocity is achieved using the well-known SIMPLE (Semi-Implicit Method for Pressure-Linked Equations) algorithm [20]. The convergence criteria were set to $10^{-9}$ for all the relative (scaled) residuals. The nominal Rayleigh numbers for most of the simulations considered here remains well above the critical limit, and under this condition the numerical round-off errors are sufficiently large to serve as initial perturbations responsible for fluid motion in the enclosure. The same numerical procedure was used in several previous studies [4–8]. Moreover, the sensitivity of the steady-state solution to the initial condition was carefully analysed for both Newtonian and Bingham cases by obtaining the same numerical results using different initial conditions (i.e. using either the conduction solution or a higher $Ra$ simulation in which convection is already significant). In addition, no hysteresis in terms of Bingham number was observed in the simulations involving yield stress fluids.

### 3.1. Governing equations

For the present study steady-state flow of an incompressible Bingham fluid is considered. The conservation equations for mass, momentum and energy for incompressible fluids under steady-state take the following form:

Mass conservation equation

$$\frac{\partial u_i}{\partial x_i} = 0 \tag{12}$$

Momentum conservation equations

$$\rho u_j \frac{\partial u_i}{\partial x_j} = -\frac{\partial P}{\partial x_i} + \rho g \delta_{i2} \beta (T - T_C) + \frac{\partial \tau_{ij}}{\partial x_j} \tag{13}$$

Energy conservation equation

$$\rho u_j c_p \frac{\partial T}{\partial x_j} = \frac{\partial}{\partial x_j}\left(k \frac{\partial T}{\partial x_j}\right) \tag{14}$$

where the cold wall temperature $T_C$ is taken to be the reference temperature for evaluating the buoyancy term $\rho g \delta_{i2} \beta (T - T_C)$ in the momentum conservation equations following several previous studies [1–15]. The stress tensor is evaluated using either Eqs. (5) and (6) (bi-viscosity approach) or Eq. (7) (Papanastasiou regularization).

In the bi-viscosity approximation to the Bingham model, the ratio of the yield viscosity ($\mu_{yield}$) to the plastic viscosity ($\mu$) was taken to be $10^4$. In order to assess the sensitivity of the value of $\mu_{yield}$, the simulations have been carried out for both $\mu_{yield} = 10^3\mu$ and $\mu_{yield} = 10^4\mu$, and the quantitative agreement between the results are found to be satisfactory for all cases (i.e. maximum deviation in the mean Nusselt number $\overline{Nu} = \int_0^L Nu dx_1/L$ is of the order of 0.5%). Given this agreement, the body of results presented in this paper are for $\mu_{yield} = 10^4\mu$: one set of results are also included for $\mu_{yield} = 10^5\mu$ to highlight the negligible effect.

### 3.2. Boundary conditions

The simulation domain is shown schematically in Fig. 1 where the two horizontal walls of a square enclosure are kept at different temperatures with the lower wall kept at higher temperature ($T_H > T_C$). The vertical walls are considered to be adiabatic in nature. Both velocity components (i.e. $u_1$ and $u_2$) are identically zero on each boundary because of the no-slip condition and impenetrability of rigid boundaries. The temperatures for cold and hot horizontal walls are specified (i.e. $T(x_2 = 0) = T_H$ and $T(x_2 = L) = T_C$). The temperature boundary conditions for the vertical insulated boundaries are given by: $\partial T/\partial x_1 = 0$ at $x_1 = 0$ and $x_1 = L$.

### 3.3. Grid Independency study

The grid independence of the results has been established based on a careful analysis of four different non-uniform meshes M1 ($20 \times 20$), M2 ($40 \times 40$), M3 ($80 \times 80$) and M4 ($160 \times 160$) the details of which are included in Table 1. For some representative simulations (Newtonian ($Bn = 0$) and $Bn = 0.25$ for $Ra = 10^5$ and $Pr = 10$) the numerical uncertainty is quantified here using Richardson's extrapolation theory [21–23]. For a primitive variable $\varphi$ the Richardson's extrapolation value is given by: $\varphi_{h=0} = \varphi_1 + (\varphi_2 - \varphi_1)/(r^p - 1)$ where $\varphi_1$ is obtained based on fine grid and $\varphi_2$ is the solution based on next level of coarse grid, $r$ is the ratio between coarse to fine grid spacings and $p$ is the theoretical order of accuracy. In this analysis the apparent order $p$ was taken to be 2. The numerical uncertainties for the mean Nusselt number $\overline{Nu}$ and the maximum non-dimensional horizontal velocity ($U_{max}$) magnitude on the vertical mid-plane of the enclosure are presented in Table 2. As seen in Table 2, the maximum numerical uncertainty between meshes remains at most 2% for $U_{max}$ in all cases. The uncertainty in $\overline{Nu}$ is considerably smaller than this value (<0.25%).

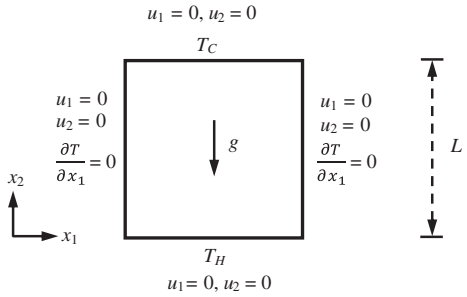


**Fig. 1.** Schematic diagram of the simulation domain.

**Table 1**
Non-dimensional minimum cell distance ($\Delta_{min,cell}/L$) and grid expansion ratio ($r$) values.

| Grid | M1 $20 \times 20$ | M2 $40 \times 40$ | M3 $80 \times 80$ | M4 $160 \times 160$ |
|---|---|---|---|---|
| $(\Delta_{min,cell}/L)$ | $4.1325 \times 10^{-3}$ | $1.8534 \times 10^{-3}$ | $8.7848 \times 10^{-4}$ | $4.3001 \times 10^{-4}$ |
| $r$ | 1.5137 | 1.2303 | 1.1092 | 1.0532 |

**Table 3**
Comparison of present simulation results for a Newtonian fluid with the results by Quertatani et al. [8] for $Pr = 0.71$.

| $Ra$ | Present study | Quertatani et al. [8] |
|---|---|---|
| $1 \times 10^3$ | 1.000 | 1.000 |
| $1 \times 10^4$ | 2.154 | 2.158 |
| $1 \times 10^5$ | 3.907 | 3.910 |
| $1 \times 10^6$ | 6.363 | 6.309 |

In addition to this grid-dependency study, mean Nusselt numbers obtained from the present numerical simulations for $Ra = 10^3$–$10^6$ at $Pr = 0.71$ for Newtonian fluids are compared with previous results [8] from the literature in Table 3. It is evident from Table 3 that the present results agree extremely well with previous numerical results by Quertatani et al. [8].The yield stress simulations have been conducted for Bingham numbers $Bn$ ranging from 0 to $Bn_{max}$ where $Bn_{max}$ is the Bingham number at which the mean Nusselt number approaches to unity (i.e. $\overline{Nu} = 1.0$) and the solution is essentially the pure-conduction result.

## 4. Scaling analysis

A scaling analysis is performed to elucidate the anticipated effects of Rayleigh number, Prandtl number and Bingham number on the Nusselt number for yield-stress fluids. The wall heat flux $q$ can be scaled as:

$$q \sim k\frac{\Delta T}{\delta_{th}} \sim h\Delta T \tag{15}$$

where the $\sim$ symbol is used to denote the equality of the order of magnitudes of the quantities on left and right hand sides of the equation in question. Eq. (15) gives rise to the following relation:

$$Nu \sim \frac{h.L}{k} \sim \frac{L}{\delta_{th}} \quad \text{or} \quad Nu \sim \frac{L}{\delta} f_2(Ra, Pr, Bn) \tag{16}$$

where the thermal boundary-layer thickness $\delta_{th}$ is related to the hydrodynamic boundary-layer thickness $\delta$ in the following manner: $\delta/\delta_{th} \sim f_2(Ra, Pr, Bn)$ where $f_2(Ra, Pr, Bn)$ is a function of Rayleigh, Prandtl and Bingham numbers (i.e. $Ra$, $Pr$ and $Bn$), which is expected to increase with increasing Prandtl number. In order to estimate the hydrodynamic boundary-layer thickness $\delta$, the equality of the order of magnitudes of the inertial and viscous forces in the vertical direction (i.e. $x_2$-direction) is considered:

$$\rho\frac{\vartheta^2}{L} \sim \frac{\tau}{\delta} \tag{17}$$

**Table 2**
Numerical uncertainty for mean Nusselt number and maximum non-dimensional horizontal velocity component on the vertical mid-plane at $Ra = 1 \times 10^5$ and $Pr = 10$ for Newtonian and Bingham ($Bn = 0.25$) fluids.

| | | $\overline{Nu}$ | | | $U_{max}$ | | |
|---|---|---|---|---|---|---|---|
| | | M2 | M3 | M4 | M2 | M3 | M4 |
| Newtonian fluid | $\phi$ | 3.861 | 3.866 | 3.869 | 77.660 | 78.256 | 78.438 |
| | $\phi_{ext}$ | | 3.870 | | | 78.499 | |
| | $e_{ext}$ (%) | 0.232 | 0.103 | 0.025 | 1.068 | 0.309 | 0.077 |
| Bingham fluid ($Bn = 0.25$) | $\phi$ | 3.572 | 3.573 | 3.574 | 61.190 | 62.126 | 62.435 |
| | $\phi_{ext}$ | | 3.5743 | | | 62.538 | |
| | $e_{ext}$ (%) | 0.065 | 0.037 | 0.009 | 2.155 | 0.659 | 0.165 |

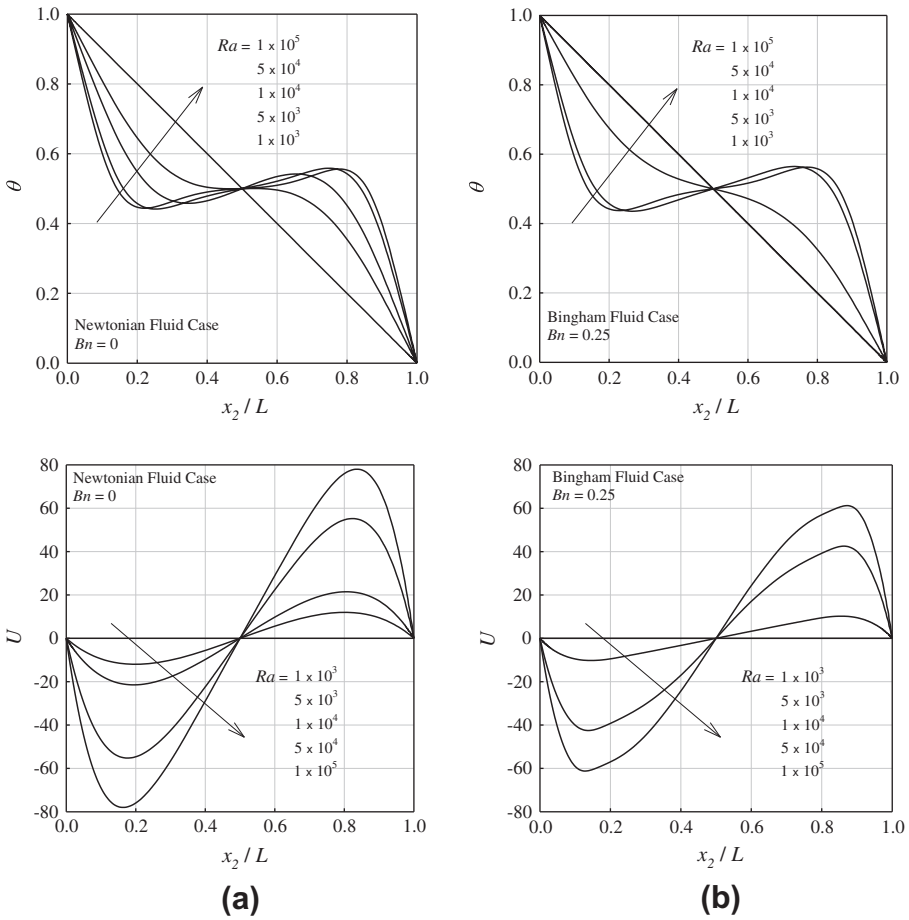


**Fig. 2.** Variations of non-dimensional temperature $\theta$ and horizontal velocity component $U$ along the vertical mid-plane (i.e. along $x_1/L = 0.5$) for different $Ra$ values at $Pr = 10$: (a) Newtonian fluid, (b) Bingham fluid ($Bn = 0.25$).

where $\vartheta$ is a characteristic velocity scale. For Bingham fluids the shear stress $\tau$ can be estimated as: $\tau \sim \tau_y + \mu\vartheta/\delta$, which upon substitution in Eq. (17) gives:

$$\rho\frac{\vartheta^2}{L} \sim \left(\tau_y + \mu\frac{\vartheta}{\delta}\right)\frac{1}{\delta} \tag{18}$$

Using Eq. (18) the hydrodynamic boundary-layer thickness can be estimated as:

$$\delta = \frac{1}{2}\frac{\tau_y L}{\rho\vartheta^2} + \frac{1}{2}\frac{L}{\rho\vartheta^2}\sqrt{\tau_y^2 + 4\rho\frac{\vartheta^3}{L}\mu}. \tag{19}$$

For natural convection the flow is induced by the buoyancy force and the equality of the order of magnitudes of inertial and buoyancy forces gives:

$$\frac{\vartheta^2}{L} \sim g\beta\Delta T. \tag{20}$$

This leads to an expression for the characteristic velocity scale:

$$\vartheta \sim \sqrt{g\beta\Delta TL} \sim (\mu/\rho L)\sqrt{Ra/Pr}, \tag{21}$$

which can be used in Eq. (19) to yield:

$$\delta \sim \frac{\mu/\rho}{\sqrt{g\beta\Delta TL}}\left[\frac{Bn}{2} + \frac{1}{2}\sqrt{Bn^2 + 4\left(\frac{Ra}{Pr}\right)^{1/2}}\right], \tag{22}$$

where $Ra$ and $Bn$ are given by Eqs. (8) and (10) respectively. This scaling gives rise to the following expression for the thermal boundary-layer thickness $\delta_{th}$:

$$\delta_{th} \sim \min\left[L, \frac{LPr^{1/2}}{f_2(Ra, Bn, Pr)Ra^{1/2}}\left[\frac{Bn}{2} + \frac{1}{2}\sqrt{Bn^2 + 4\left(\frac{Ra}{Pr}\right)^{1/2}}\right]\right]. \tag{23}$$

The above expression accounts for the fact that the thermal boundary-layer thickness becomes of the order of the enclosure size $L$ under very high values of $Bn$ when the Bingham fluid acts essentially as a solid material. Eq. (23) suggests that $\delta_{th}$ decreases with increasing $Ra$, which acts to increase the wall heat flux. Substitution of Eq. (23) into Eq. (16) yields:

$$\overline{Nu} \sim Max\left[1.0, \frac{(Ra/Pr)^{1/2}}{\left[\frac{Bn}{2} + \frac{1}{2}\sqrt{Bn^2 + 4\left(\frac{Ra}{Pr}\right)^{1/2}}\right]} f_2(Ra, Pr, Bn)\right]. \tag{24}$$

The scaling predictions provide useful insight into the anticipated behaviour of the mean Nusselt number $\overline{Nu}$ in response to variations of $Ra$, $Pr$ and $Bn$. The analysis suggests that $\overline{Nu}$ is expected to decrease with increasing $Bn$ for a given value of $Ra$ whereas $\overline{Nu}$ increases with increasing $Ra$ for a given value of $Bn$. It is also important to note that the Nusselt number behaviour for Newtonian fluids can be obtained by setting $Bn = 0$ in Eq. (24).

## 5. Results & discussion

### 5.1. Rayleigh number effects

The variations of non-dimensional temperature $\theta = (T - T_C)/(T_H - T_C)$ and horizontal velocity component $U = u_1 L/\alpha$ along the vertical mid-plane for different values of nominal Rayleigh number

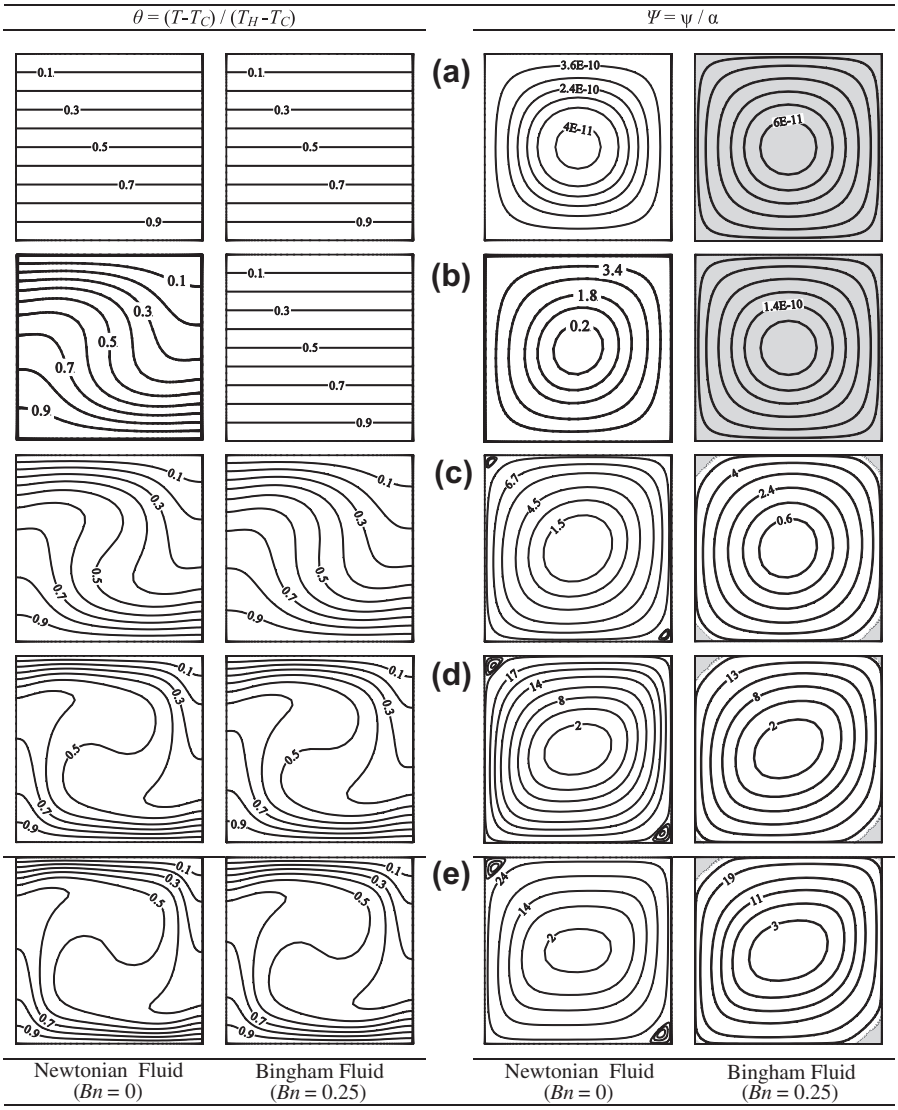


**Fig. 3.** Contours of non-dimensional temperature $\theta$ and stream function $\Psi$ for Newtonian fluid and Bingham fluid ($Bn = 0.25$) at $Pr = 10$ for $Ra =$ (a) $1 \times 10^3$, (b) $5 \times 10^3$, (c) $1 \times 10^4$, (d) $5 \times 10^4$ and (e) $1 \times 10^5$.

are shown in Fig. 2 for Newtonian (i.e. $Bn = 0$) and Bingham (i.e. $Bn = 0.25$) fluids at $Pr = 10$. The distributions of the vertical velocity component is not shown as the horizontal and vertical velocity components remain of the same order of magnitude in square enclosures in order to satisfy the continuity relation (i.e. $u_1/L \sim u_2/L$). As a consequence of fluid motion the distributions of $\theta$ with $x_2/L$ become increasingly non-linear with increasing $Ra$. The extent of non-linearity of the $\theta$ distribution increases with strengthening of convective transport within the enclosure. Such an effect is confirmed from the distributions of $U$, which show that the magnitude of $U$ increases with increasing Rayleigh number. These trends are consistent with the velocity scaling given by Eq. (21), which indicates that $U$ increases with increasing $Ra$ for a given value of $Pr$. Comparing the distributions of $U$ for $Bn = 0$ and $Bn = 0.25$ cases reveal that the velocity magnitudes in the Bingham fluid cases are smaller than in the case of Newtonian fluids. The effects of flow resistance are stronger in Bingham fluids than in Newtonian fluids which gives rise to a smaller magnitude of $U$ in the $Bn = 0.25$ case than in the Newtonian (i.e. $Bn = 0$) case. It is clearly evident from Fig. 2 that heat transfer takes place predominantly due to thermal conduction for small values of Rayleigh number (e.g. $Ra = 1000$) for both Newtonian and Bingham fluids, as the density change due to temperature variation remains too weak to induce fluid motion to impart any influence on thermal transport. Under this circumstance, the heat transfer takes place solely due to thermal conduction, which gives rise to a linear distribution of $\theta$ with $x_2/L$ for small values of nominal Rayleigh number $Ra$. The aforementioned physical descriptions can be verified from the contours of $\theta$ and non-dimensional stream function $\Psi = \psi/\alpha$ shown in Fig. 3. It is clear from Fig. 3 that the effects of convection are felt at relatively higher Rayleigh number for Bingham fluids than in the case of Newtonian fluids (see $Ra = 5 \times 10^3$ cases for example) due to stronger flow resistance in Bingham fluids. This is also reflected in the smaller magnitude of $\Psi$ in Bingham fluids than in Newtonian fluids (see Fig. 3). For small values of $Ra$ the isotherms remain parallel to the horizontal walls indicating predominantly conduction mode of heat transfer. However, the isotherms become curved with the strengthening of convective transport in the enclosure. As the circulation pattern remain qualitatively similar at a given Rayleigh number, the isotherms for both Newtonian and $Bn = 0.25$ cases look similar. The "unyielded" zones according to the criterion proposed by Mitsoulis [24] (i.e. zones of fluid where $\sqrt{\tau_{12}\tau_{12}} \leqslant \tau_y$) are also shown in Fig. 3 for $Bn = 0.25$. It is worth noting that these zones aren't truly "unyielded" as indicated by Mitsoulis and Zisis

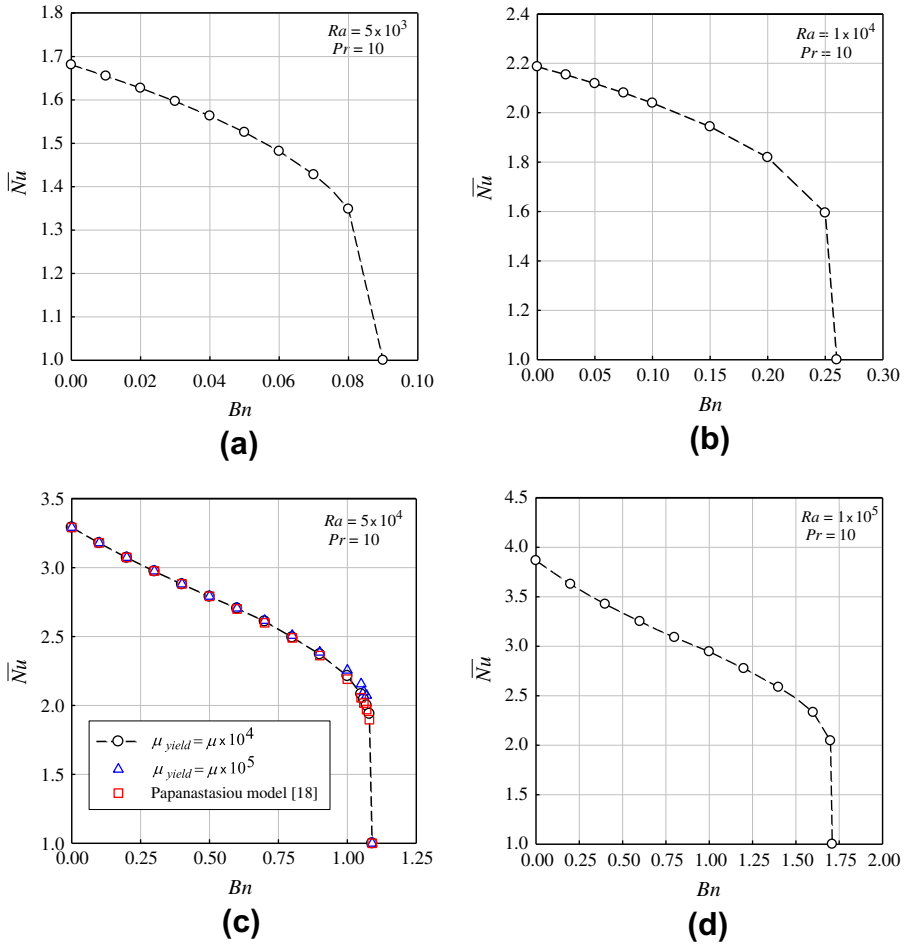


**Fig. 4.** The interrelation between the mean Nusselt number $\overline{Nu}$ and Bingham number $Bn$ at $Pr = 10$ for $Ra =$ (a) $1 \times 10^3$, (b) $5 \times 10^3$, (c) $1 \times 10^4$, (d) $5 \times 10^4$ and (e) $1 \times 10^5$.

[25]. In the results shown in Fig. 3 a bi-viscosity regularisation is employed to account for the Bingham fluid flow so there will always be extremely slowly moving fluid flow within these essentially very high viscosity regions, which Mitsoulis and Zisis [25] termed as the "apparently unyielded regions (AUR)". It is important to indicate that the small islands of AUR alter with increasing values of $\mu_{yield}$ (shown in Fig. 3 for $\mu_{yield} = 10^4\mu$) while the mean Nusselt number, and the streamfunction are independent of $\mu_{yield}$ for $\mu_{yield} \geqslant 10^3\mu$. For a given value of $\tau_y$ the AURs, which satisfy $\sqrt{\tau_{12}\tau_{12}} \leqslant \tau_y$, are expected to shrink with an increase in $\mu_{yield}$. As the AURs are dependent on the precise choice of $\mu_{yield}$ and the value of $\overline{Nu}$ remains independent of the shape and size of AURs for $\mu_{yield} \geqslant 10^3\mu$, their effects on heat transfer are clearly minimal.

The variation of the mean Nusselt number $\overline{Nu}$ with $Bn$ for different values of $Ra$ at $Pr = 10$ are shown in Fig. 4 (the cases corresponding to $Ra = 10^3$ are not shown because the mean Nusselt number $\overline{Nu}$ remains equal to unity for all fluids). The results shown in Fig. 4 are primarily obtained from the bi-viscosity regularisation but the use of the exponential form of the Bingham model (due to Papanastasiou [18]) was found to give virtually identical results as shown in Fig. 4c. Fig. 4c also highlights the negligible effect of further increasing the $\mu_{yield}$ parameter in the bi-viscosity model. The variation in Nusselt number between the regularisation methods for nominally identical conditions was usually smaller than 0.1% and small differences became apparent only at large Bingham numbers, when the Nusselt number approaches unity, (still less than 3% in $\overline{Nu}$). These differences are, for all practical purposes, unimportant for the following discussion. Fig. 4 indicates that $\overline{Nu}$ decreases with increasing $Bn$, which is consistent with the scaling estimate given by Eq. (24). The weaker convection strength in the Bingham fluids than in the case of Newtonian fluids results in a smaller value of $\overline{Nu}$ in Bingham fluids. An increase in $Bn$ implies that higher stress needs to be created to induce fluid motion and thus thermal convection within the enclosure. This increased flow resistance at higher values of Bingham number $Bn$ gives rise to weaker thermal convection in the enclosure, which is reflected in the small values of $\overline{Nu}$ for high values of $Bn$. It can be seen from Fig. 4 that $\overline{Nu}$ at a given set of values of $Ra$ and $Pr$ decreases with increasing $Bn$ before dropping to $\overline{Nu} = 1.0$ at a Bingham number $Bn_{\max}$ such that $\overline{Nu}$ remains equal to unity for $Bn \geqslant Bn_{\max}$. The heat transfer for $Bn \geqslant Bn_{\max}$ takes place due to thermal conduction which is reflected in the unity value of mean Nusselt number (i.e. $\overline{Nu} = 1.0$), which can be confirmed from Fig. 5 where the variations of $\theta_{RMS}$ and $U_{RMS}$ with $Bn$ are presented. The quantity $\varphi_{RMS}$ is the root-mean-square (rms) value of a primitive variable $\varphi$ with respect to the pure-conduction solution (i.e. $U = 0$ and $\theta = x_2/L$). The quantity $\varphi_{RMS}$ is evaluated as: $\phi_{RMS} = \sqrt{\sum_{cv}(\phi_{cv} - \phi_{cv}^{cond})^2 \Delta V_{cv}/V_{domain}}$ where $\Delta V_{cv}$ is the volume of the control volume in the context of the finite-volume technique, $V_{domain}$ is the domain volume, $\varphi_{cv}$ is the quantity in question at the centre of the control volume, $\varphi_{cv}^{cond}$ is the quantity in question at the centre of the control volume according to the pure-conduction solution. It is evident from Fig. 5 that both $\theta_{RMS}$ and $U_{RMS}$ decrease with increasing $Bn$ for a given set of values of $Ra$ and $Pr$ suggesting that the steady state solution approaches to the steady-state pure-conduction solution with

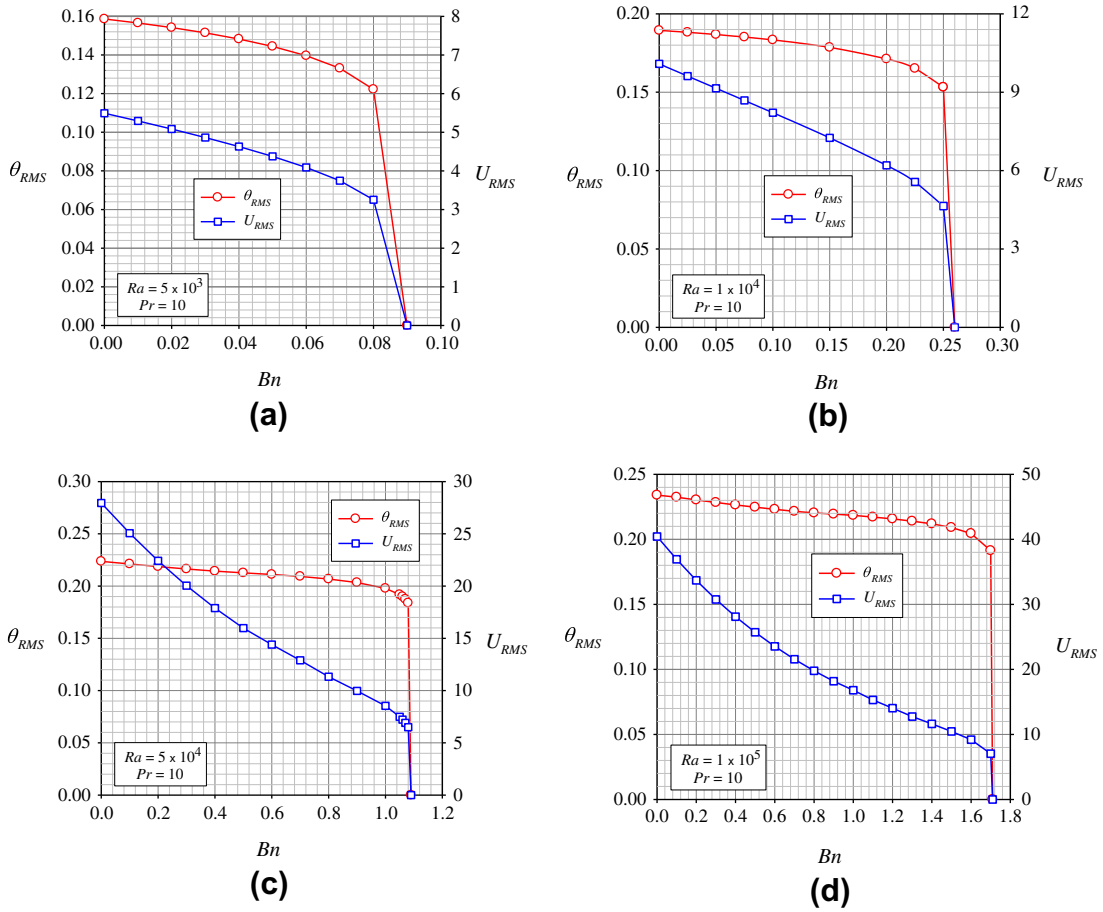


**Fig. 5.** Variations of $\theta_{RMS}$ and $U_{RMS}$ with $Bn$ at $Pr = 10$ for $Ra =$ (a) $1 \times 10^3$, (b) $5 \times 10^3$, (c) $1 \times 10^4$, (d) $5 \times 10^4$ and (e) $1 \times 10^5$.

increasing $Bn$. The weakening of convection strength with increasing $Bn$ is also evident from the decrease in $U_{RMS}$ with increasing $Bn$. A comparison between Figs. 4 and 5 reveals that $\theta_{RMS}$ and $U_{RMS}$ assume negligible values for $Bn \geqslant Bn_{max}$ indicating a purely conduction-driven thermal transport which is reflected in the unity value of the mean Nusselt number $\overline{Nu}$.

Fig. 4 shows that the mean Nusselt number $\overline{Nu}$ increases with increasing $Ra$ for a given set of values of $Pr$ and $Bn$ for $Bn < Bn_{max}$, which is also consistent with the scaling estimates given by Eq. (24). An increase in $Ra$ gives rise to strengthening of convection for a given set of values of $Pr$ and $Bn$ for $Bn < Bn_{max}$ and this is reflected in the high values of $\overline{Nu}$ for high $Ra$. The strengthening of fluid motion with increasing $Ra$ can also be confirmed from Fig. 5, which shows an increase in $U_{RMS}$ with increasing $Ra$ for a given set of values of $Bn$ and $Pr$. Stronger fluid flow at higher values of Rayleigh number can overcome the flow resistance up to greater values of Bingham number which gives rise to an increase in $Bn_{max}$ with increasing $Ra$ for a given value of $Pr$.

### 5.2. Bingham number effects

In order to demonstrate the effects of Bingham number on natural convection of Bingham fluids in square enclosures, the variations of non-dimensional temperature $\theta$ and horizontal velocity component $U$ along the vertical mid-plane for different values of $Bn$ at $Ra = 10^4$ and $10^5$ are shown in Fig. 6 for $Pr = 10$. It can be seen from Fig. 6 that the variation of $\theta$ with $x_2/L$ becomes increasingly linear for increasing $Bn$ as the convective strength diminishes with increasing Bingham number and a tendency towards the linear variation of $\theta$ with $x_2/L$ indicates that the relative contribution of thermal conduction to the overall heat transfer increases with increasing $Bn$. The diminishing strength of convection with increasing $Bn$ can be confirmed from the decreasing magnitudes of $U$ with increasing $Bn$. The isotherms are more non-linear at $Ra = 10^5$ than in the $Ra = 10^4$ case due to stronger convection at higher values of Rayleigh number which can further be confirmed from the higher magnitudes of $U$ in the $Ra = 10^5$ case than in the $Ra = 10^4$ case. The above behaviour can be substantiated from the contours of $\theta$ and $\Psi$ at $Ra = 10^4$ and $10^5$ in Fig. 7 for $Pr = 10$. It can be seen from Fig. 7 that the magnitude of $\Psi$ decreases with increasing Bingham number due to weakening of fluid motion and this is reflected in the increased size of AURs for higher values of $Bn$. At high values of $Bn$ the whole enclosure becomes an AUR and under this condition the fluid flow becomes too weak to influence the heat transfer and thus the heat transfer takes place solely due to thermal conduction. This pure-conduction limit is reflected in the parallel horizontal isotherms in Fig. 7. The isotherms become increasingly curved with decreasing $Bn$ due to strengthening of convective transport.

The strengthening of flow resistance, which gives rise to weakening of convective transport, leads to a concomitant decrease of $\overline{Nu}$ with increasing $Bn$ as shown in Fig. 4 as has been observed previously in the context of differentially heated vertical sidewalls in square enclosures [13–15]. However, it is worth noting that the variation of $\overline{Nu}$ with $Bn$ in rectangular enclosures with differentially-heated vertical sidewalls (see Fig. 12 of Ref. [13] for example) is both quantitatively and qualitatively different from the variation

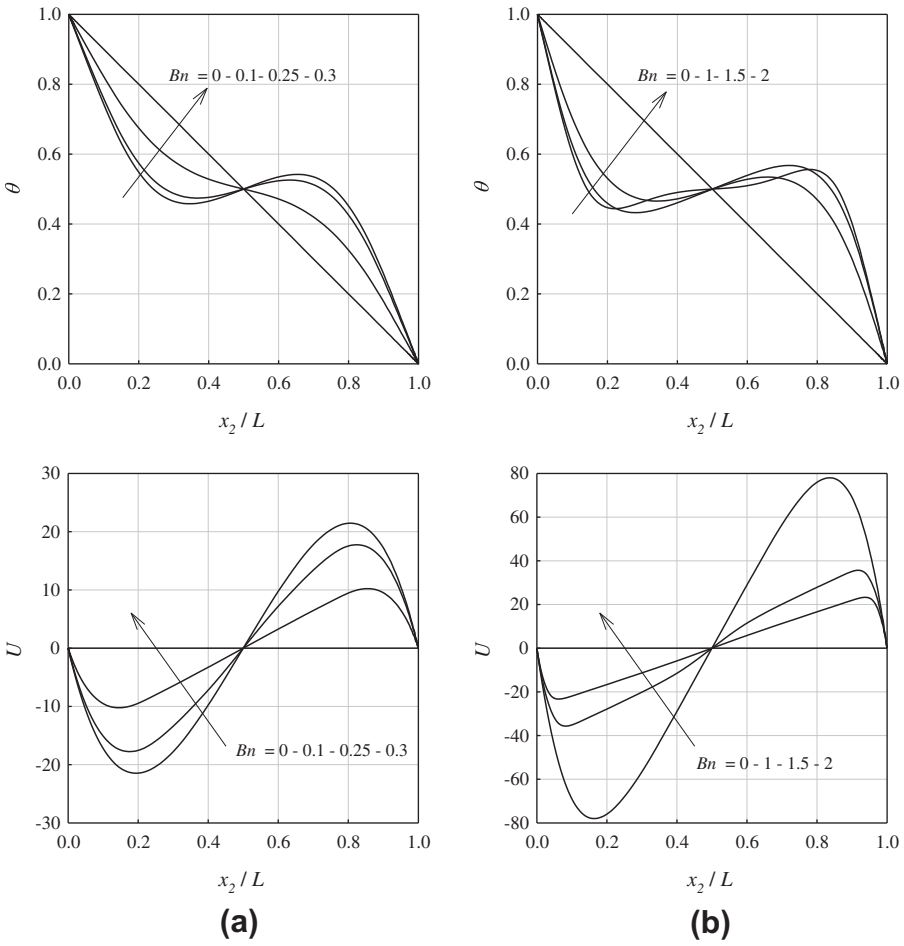


**Fig. 6.** Variations of non-dimensional temperature $\theta$ and horizontal velocity component $U$ along the vertical mid-plane (i.e. along $x_1/L = 0.5$) for Bingham fluids at $Pr = 10$: for $Ra$ = (a) $1 \times 10^4$, (b) $1 \times 10^5$.

of $\overline{Nu}$ with $Bn$ in the RB configuration for the same nominal values of $Ra$ and $Pr$. In the case of differentially-heated vertical sidewalls $\overline{Nu}$ decreases gradually from the Newtonian value (i.e. $Bn = 0$) with increasing $Bn$ and eventually settles to unity. In contrast, the variation of $\overline{Nu}$ with $Bn$ in Fig. 4 shows a gradual decrease from the Newtonian value with increasing $Bn$ before exhibiting a rapid drop of $\overline{Nu}$ to unity at $Bn = Bn_{max}$.

### 5.3. Prandtl number effects

The effects of $Pr$ on the mean Nusselt number $\overline{Nu}$ for Newtonian fluids (i.e. $Bn = 0$) is shown in Fig. 8, which shows $\overline{Nu}$ slightly increases between $Pr = 0.1$ and 1.0 but the change in $\overline{Nu}$ is marginal between $Pr = 1.0$ and 1000. The heat transfer characteristics in the present configuration depend on the relative strengths of inertial, viscous and buoyancy forces. For small values of $Pr$ the thermal boundary-layer thickness remains much greater than the hydrodynamic boundary-layer thickness and thus the inertial and buoyancy forces principally govern the thermal transport. In contrast, for large values of $Pr$ the hydrodynamic boundary-layer thickness remains much greater than the thermal boundary-layer thickness thus the transport characteristics are primarily governed by buoyancy and viscous forces (see the scaling analysis by Bejan [26]). For $Pr \ll 1$, an increase in $Pr$ decreases the thermal boundary-layer thickness in comparison to the hydrodynamic boundary-layer thickness, which acts to increase the heat flux which is reflected in the increasing Nusselt number. In the case of $Pr \gg 1$, a change in Prandtl number modifies the relative balance between viscous and buoyancy forces so the heat transport in the thermal boundary layer gets only marginally affected. This marginal modification is reflected in the weak Prandtl number dependence of $\overline{Nu}$ for large values of $Pr$ (i.e. $Pr \gg 1$) observed in Fig. 8. It is also evident from Fig. 8 that the present numerical results for Newtonian fluids are in good agreement with previous results [8,27] for $Pr = 0.71$. In the present study a correlation for the mean Nusselt number $\overline{Nu}$ for Newtonian fluids is proposed in the following manner:

$$\overline{Nu} = aRa^m \left(\frac{Pr}{1+Pr}\right)^n. \tag{25i}$$

The values of the coefficients $a$, $m$ and $n$ were determined by an iterative minimisation function of a commercial software package which provides the following values:

$$a = 0.178, \quad m = 0.269, \quad n = 0.02. \tag{25ii}$$

For the parameters given by Eq. (25ii), the correlation of Eq. (25i) satisfactorily captures the variation of $\overline{Nu}$ with $Pr$ for Newtonian fluids (i.e. a maximum relative error 4.65% with a mean relative error 2.65% for $10^3 \leqslant Ra \leqslant 10^5$ and $0.1 \leqslant Pr \leqslant 10^3$). It is worth noting that setting $Bn = 0$ in Eq. (24) yields a scaling estimate of $\overline{Nu} \sim (Ra/Pr)^{0.25} f_2(Ra, Pr)$ which is in excellent agreement with the correlation given by the scaling analysis (i.e. Eq. (25i)). Given the simplicity of the scaling argument the slight disagreement between the exponents of Rayleigh number (i.e. 0.269 as opposed to 0.25) is not surprising.

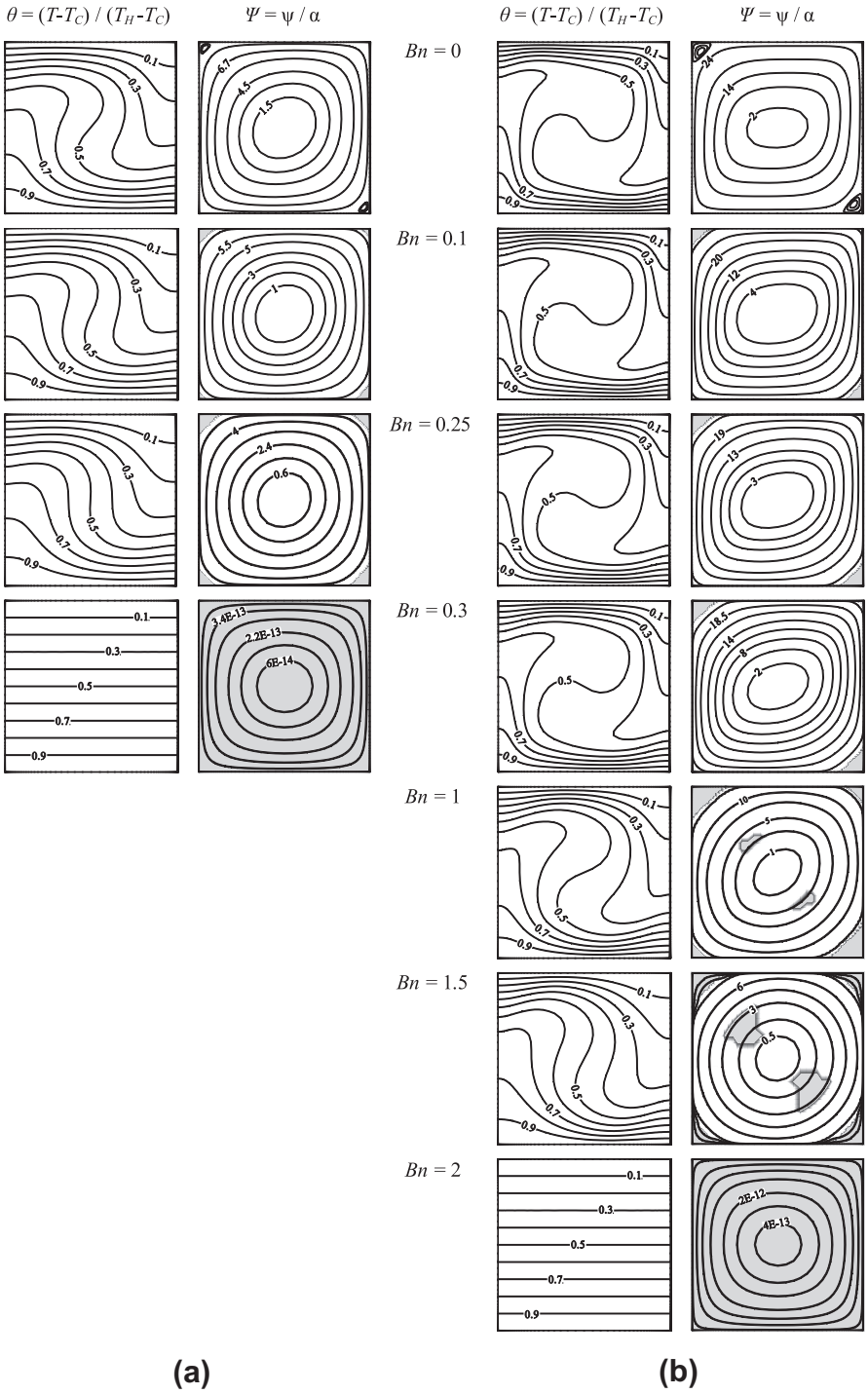


**Fig. 7.** Contours of non-dimensional temperature $\theta$ and stream function $\Psi$ for Bingham fluids at $Pr = 10$ for $Ra =$ (a) $1 \times 10^4$, (b) $1 \times 10^5$.

The variations of $\overline{Nu}$ with $Bn$ for different Prandtl numbers at $Ra = 10^4$ are shown in Fig. 9a, which show that unlike Newtonian fluids the mean Nusselt number $\overline{Nu}$ decreases with increasing $Pr$ for large values of $Bn$. However, the mean Nusselt number $\overline{Nu}$ increases with increasing $Pr$ for very small values of $Bn$, which is consistent with the behaviour obtained for Newtonian fluids (see Fig. 8). Moreover, the value of Bingham number $Bn_{max}$ for which $\overline{Nu}$ approaches to unity decreases with increasing $Pr$. The same qualitative behaviour is also observed for other values of $Ra$. This variation clearly demonstrates that $Bn_{max}$ depends on $Pr$ for a given value of $Ra$, which can be confirmed from Fig. 9b where the values of $Bn_{max}$ are estimated here by carrying out simulations and identifying the Bingham number at which $\overline{Nu}$ assumes a value of 1.01 (i.e. $\overline{Nu} = 1.01$). As the Nusselt number variation close to $Bn_{max}$ is so rapid – see Fig 4d for example where $\overline{Nu}$ decreases by a factor of two with a 5% increase in Bingham number – this criteria allows a very accurate determination of $Bn_{max}$ (cf. sidewall heating case results [13–15] where estimating $Bn_{max}$ is much more difficult).

From the foregoing it can be concluded that the effects of $Pr$ on natural convection at a given value of $Ra$ are not fully independent of $Bn$. This inference is an artefact of how the nominal $Ra$ is defined in the present analysis (see Eq. (8)). In the case of natural convec-

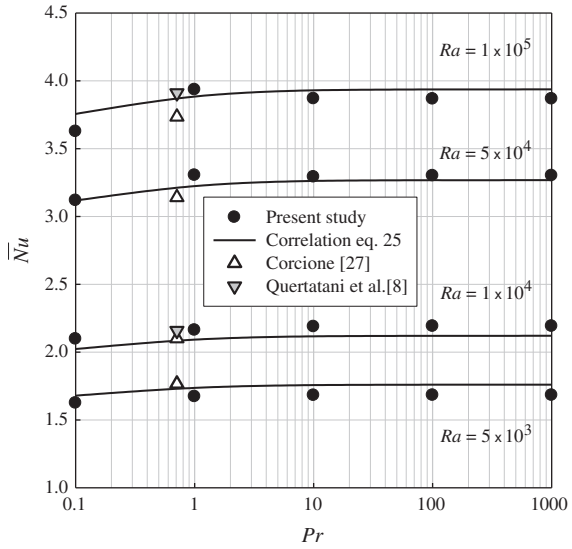


**Fig. 8.** Variation of mean Nusselt number $\overline{Nu}$ with Rayleigh $Ra$ and Prandtl $Pr$ numbers for Newtonian fluids.

tion in Bingham fluids an effective viscosity $\mu_{eff}$ can be estimated as:

$$\mu_{eff} = \tau_y/\dot{\gamma} + \mu, \tag{26}$$

which can be scaled as:

$$\mu_{eff} \sim \tau_y \delta/\vartheta + \mu. \tag{27}$$

Using Eq. (22) in Eq. (27) gives rise to:

$$\mu_{eff} \sim \mu\left\{Bn\left[\frac{Bn\mu}{2\rho\vartheta L} + \frac{\mu}{2\vartheta L\rho}\sqrt{Bn^2 + 4\frac{\rho\vartheta L}{\mu}}\right]\right\} + \mu. \tag{28}$$

Using velocity scale $\vartheta \sim \sqrt{g\beta\Delta TL}$ gives:

$$\mu_{eff}/\mu \sim \left\{Bn\left[\frac{Bn}{2Gr^{1/2}} + \frac{1}{2Gr^{1/2}}\sqrt{Bn^2 + 4Gr^{1/2}}\right]\right\} + 1. \tag{29}$$

Based on Eq. (29) an effective Grashof number $Gr_{eff}$ can be defined as:

$$Gr_{eff} = \frac{\rho^2 g\beta\Delta TL^3}{\mu_{eff}^2} = Gr\left[\left\{Bn\left[\frac{Bn}{2Gr^{1/2}} + \frac{1}{2Gr^{1/2}}\sqrt{Bn^2 + 4Gr^{1/2}}\right]\right\} + 1\right]^{-2}. \tag{30}$$

The variation of $Gr_{eff}$ with $Pr$ according to Eq. (30) is shown in Fig. 10 for different values of $Bn$, which suggests that the effective Grashof number decreases with increasing $Pr$ for a given value of $Ra$ and this reduction in $Gr_{eff}$ becomes increasingly rapid with increasing values of $Bn$. The effects of the buoyancy force become progressively weak in comparison to the viscous effects with increasing $Pr$ for large values of $Bn$ when $Ra$ is held constant. This reduced strength of buoyancy force relative to the viscous force gives rise to a weakening of convective transport which acts to decrease $\overline{Nu}$ with increasing $Pr$. This effect is relatively weak for small values of $Bn$ where an increase in Prandtl number acts to reduce the thermal boundary-layer thickness which in turn acts to increase the heat-transfer rate as discussed earlier in the context of Newtonian fluids. By contrast, for large values of $Bn$ the effects of thinning of the thermal boundary-layer thickness with increasing $Pr$ are overcome by the reduction of convective transport strength due to a smaller value of the effective Grashof number. This reduction in strength of convective transport gives rise to a decrease in

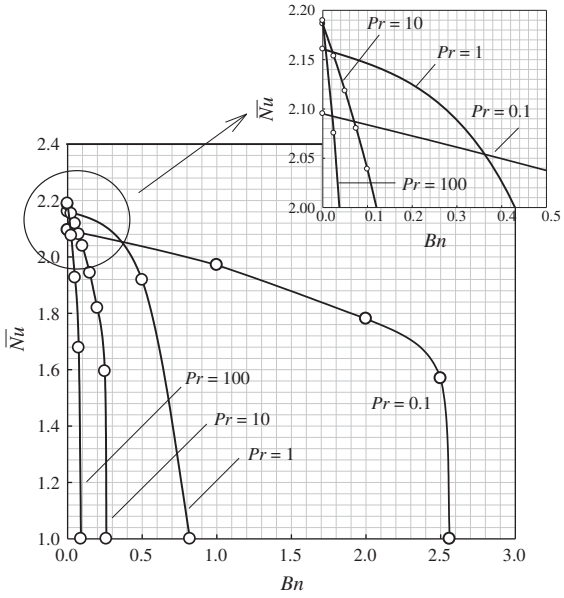


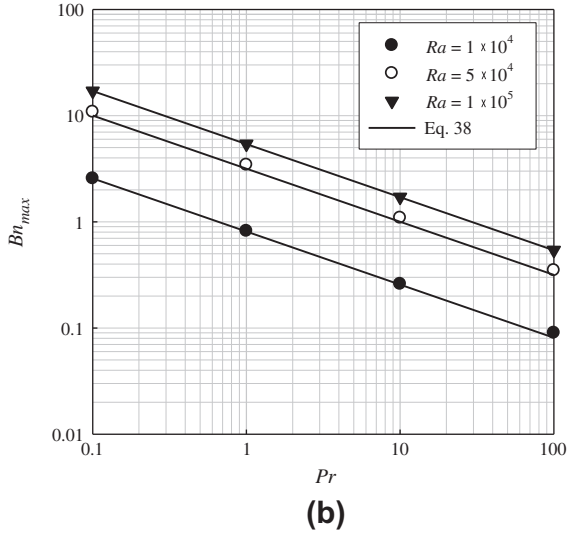


**Fig. 9.** (a) Variations of mean Nusselt number $\overline{Nu}$ with Prandtl number for Bingham fluids at $Ra = 10^4$, (b) Variation of $Bn_{max}$ for different values of $Ra$ and $Pr$.

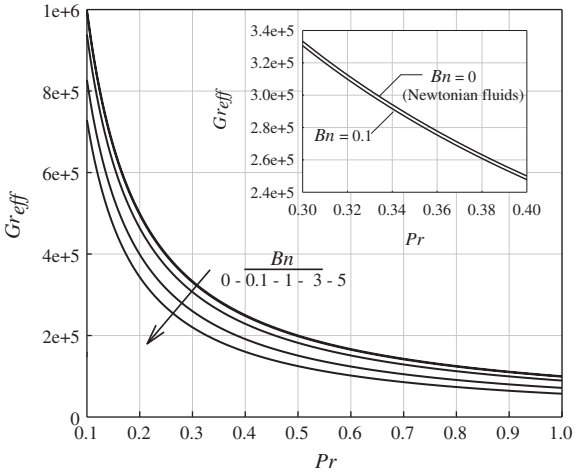


**Fig. 10.** Variation of effective Grashof number $Gr_{eff}$ with Prandtl number $Pr$ at $Ra = 10^5$.

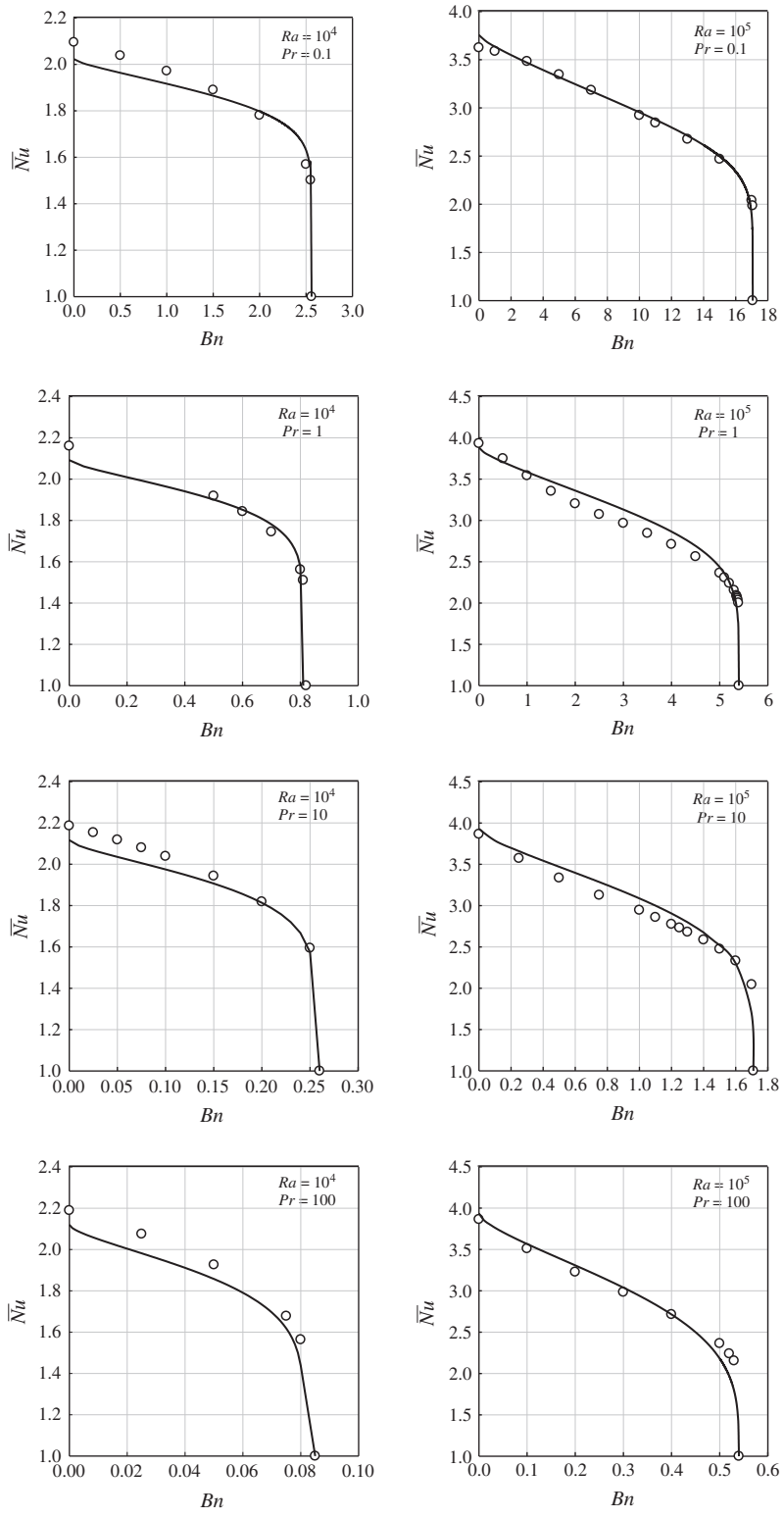


**Fig. 11.** Comparison of the prediction of the correlation (−) given by Eq. (34) and simulation results (○).

$\overline{Nu}$ with increasing values of $Pr$ (for a given value of $Ra$) when the Bingham number attains large values. Eventually this gives rise to smaller values of $Bn_{max}$ for higher $Pr$ values as shown in Fig. 9a (for constant $Ra$). As a consequence $Bn_{max}$ depends on both Rayleigh and Prandtl numbers, and $Bn_{max}$ increases with increasing Rayleigh number for a given value of Prandtl number, whereas it decreases with increasing Prandtl number for a given value of Rayleigh number as shown in Fig. 9b.

According to Eq. (27) an effective Rayleigh number can be defined as: $Ra_{eff} = \rho g \beta \Delta T L^3 / \mu_{eff} \alpha \sim Ra_{CWT} / [Bn(\delta/L) + 1]$. It has been demonstrated in Eq. (22) that $\delta$ increases with increasing $Bn$ for a given set of values of nominal Rayleigh and Prandtl numbers. This expression suggests that $Ra_{eff}$ decreases with increasing $Bn$ for a given set of values of $Ra$ and $Pr$ and convection ultimately stops once $Ra_{eff}$ drops below a critical limit where heat transfer takes place purely due to thermal conduction. This effect is reflected in the

sudden drop of $\overline{Nu}$ to unity for values close to $Bn_{max}$ in Figs. 4 and 9a.

The value of $Bn_{max}$ can be estimated using $\overline{Nu} = 1 \sim L/\delta \times f_2(Ra, Pr, Bn)$, which leads to the following expression according to Eq. (22):

$$f_2(Ra, Pr, Bn_{max}) \frac{Ra^{1/2}}{Pr^{1/2}} \sim \left[ \frac{Bn_{max}}{2} + \frac{1}{2} \sqrt{Bn_{max}^2 + 4\left(\frac{Ra}{Pr}\right)^{1/2}} \right], \quad (31)$$

which can be manipulated to yield:

$$Bn_{max} \sim f_2(Ra, Pr, Bn_{max}) \frac{Ra^{1/2}}{Pr^{1/2}} - \frac{1}{f_2(Ra, Pr, Bn_{max})}. \quad (32)$$

Eq. (32) demonstrates that $Bn_{max}$ depends on both $Ra$ and $Pr$, which is consistent with the simulation results. It is worth noting that the buoyancy force is expected to be of the same order of the force induced by yield stress when the fluid is about to yield. The equilibrium of buoyancy and yield stress effects under the aforementioned condition gives rise to the following relation:

$$\rho g \beta \Delta T \sim \frac{\tau_y}{\delta} \sim \frac{\tau_y}{L f_2}. \quad (33)$$

The above relation can further be rewritten in terms of Oldroyd number as: $B \sim f_2$ when the fluid is about to yield (consistent with the findings in Ref. [2]).

### 5.4. Correlation for $\overline{Nu}$

Guided by the scaling estimate given by Eq. (24) a correlation for the mean Nusselt number $\overline{Nu}$ is proposed here in the ranges given by $0.1 \leqslant Pr \leqslant 100$, $10^3 \leqslant Ra \leqslant 10^5$ and $0 \leqslant Bn \leqslant Bn_{max}$:

$$\overline{Nu} = 1 + \frac{ARa^{1/2}}{\left[\frac{Bn}{2} + \frac{1}{2}\sqrt{Bn^2 + 4\left(\frac{Ra}{Pr}\right)^{1/2}}\right]} \left[1 - \left(\frac{Bn}{Bn_{max}}\right)^{0.6}\right]^b \quad (34)$$

$$\lim_{Bn \to Bn_{max}} \overline{Nu} = 1 + \frac{A.Ra^{1/2}}{\left[\frac{Bn_{max}}{2} + \frac{1}{2}\sqrt{Bn_{max}^2 + 4\left(\frac{Ra}{Pr}\right)^{1/2}}\right]} \left[1 - \left(\frac{Bn_{max}}{Bn_{max}}\right)^{0.6}\right]^b = 1.0 \quad (35)$$

where $A$, $b$ and $Bn_{max}$ are input parameters in the correlation. The parameter $A$ needs to be chosen in such a manner that Eq. (34) becomes identically equal to Eq. (25i) when the Bingham number $Bn$ goes to zero (i.e. Newtonian fluid). This gives rise to the following expression for $A$:

$$A = aRa^{m-0.25} \frac{Pr^{n-0.25}}{(1+Pr)^n} - \frac{1}{Ra^{0.25} Pr^{0.25}}. \quad (36)$$

The simulation data indicates that the parameter $b$ depends on both $Ra$ and $Pr$ and it has been found that the variation of $b$ with $Ra$ and $Pr$ can be accurately expressed with the help of the following power-law:

$$b = 0.025 Ra^{0.171} Pr^{0.095}. \quad (37)$$

It has been discussed earlier that $Bn_{max}$ is dependent on $Ra$ and $Pr$ and here the value of $Bn_{max}$ is estimated by fitting the simulation results:

$$Bn_{max} = [0.0019 \ln(Ra) - 0.0128] Ra^{0.55} Pr^{-0.50}. \quad (38)$$

The prediction of $Bn_{max}$ according to Eq. (38) is compared to the corresponding values obtained from simulation results in Fig. 9b and a satisfactory agreement is obtained. The scaling relation given by Eq. (32) shows that $Bn_{max}$ is expected to have a $\sqrt{Ra/Pr}$ dependence and the empirical relation given by Eq. (38) is in remarkable agreement with the expected behaviour of $Bn_{max}$ predicted by Eq. (32). According to Eq. (38) the Oldroyd number $B_{max} = Bn_{max}\sqrt{Pr/Ra}$ scales as: $B_{max} \sim [0.0019 \ln(Ra) - 0.0128] Ra^{0.05}$. As $Bn$ approaches to $Bn_{max}$ the strength of convective transport within the enclosure becomes too weak to impart any significant influence on heat transfer to give rise to a significantly non-unity $\overline{Nu}$ despite the fluid being yielded in some regions. By contrast, the equilibrium is maintained between yield stress and buoyancy induced stresses when the fluid is about to yield (see the differences between Eqs. (31) and (33)). The present computational results demonstrate that $B_{max} = Bn_{max}\sqrt{Pr/Ra}$ varies with Rayleigh number and is not constant for all cases (although it remains of the same order varying at most by a factor of 5).

The predictions of the correlation given by Eq. (34) is compared with the simulation results in Fig. 11, which demonstrates that the correlation given by Eq. (34) satisfactorily captures both qualitative and quantitative variations of $\overline{Nu}$ with $Bn$ for the range of $Ra$ and $Pr$ analysed in this study. However, the correlation given by Eq. (34) underpredicts $\overline{Nu}$ for small values of $Bn$ for $Ra = 10^4$ and this disagreement originates principally due to the limitation of the correlation of the Newtonian fluids (Eq. (25i)) in predicting $\overline{Nu}$ for small values of $Ra$ (see Fig. 8), which in turn affects the prediction of Eq. (34) through the value of $A$.

## 6. Conclusions

In this study, steady laminar natural convection of yield-stress fluids obeying the Bingham model in a square enclosure with differentially heated horizontal walls with the bottom wall at higher temperature has been numerically analysed. The effects of nominal Rayleigh number $Ra$, Prandtl number $Pr$ and Bingham number $Bn$ on momentum and thermal transport have been investigated in detail.

The mean Nusselt number $\overline{Nu}$ is found to increase with increasing values of the Rayleigh number for both Newtonian and Bingham fluids but the Nusselt numbers obtained for Bingham fluids are smaller than those obtained in the case of Newtonian fluids with the same numerical values of nominal Rayleigh number. It is found that the mean Nusselt number for Bingham fluids decreases with increasing Bingham number, and, for large values of Bingham number (i.e. $Bn \geqslant Bn_{max}$), the value of mean Nusselt number rapidly approaches unity (i.e. $\overline{Nu} = 1$) as thermal conduction becomes the dominant mode of heat transfer. The conduction-dominated regime occurs at large values of $Bn$ for increasing values of $Ra$ as the convective transport strengthens with increasing Rayleigh number. The variations of $\overline{Nu}$ with respect to $Bn$ in this configuration are found to be markedly different in comparison to the corresponding variations in the case of differentially-heated vertical sidewalls for the same nominal values of $Ra$ and $Pr$. In the case of differentially-heated side walls $\overline{Nu}$ decreases gradually with increasing $Bn$ and eventually assumes a value equal to unity for large values of $Bn$, whereas a gradual reduction in $\overline{Nu}$ from the Newtonian value (i.e. $Bn = 0$) with increasing $Bn$ is followed by a sudden drop in $\overline{Nu}$ to unity for the enclosures with differentially heated horizontal walls with bottom surface at higher temperature. The mean Nusselt number $\overline{Nu}$ increases weakly with increasing $Pr$ for small values of Prandtl number in the case of Newtonian fluids but the mean Nusselt number remains insensitive to the change in Prandtl number for $Pr \geqslant 10$. For low Bingham number flows (for a given value of the Rayleigh number) the mean Nusselt number is found to increase with increasing Prandtl number but the opposite behaviour was observed for large values of the Bingham number. The relative strengths of buoyancy, inertial and viscous forces are shown to be responsible for this non-monotonic Prandtl number dependence of the mean Nusselt number $\overline{Nu}$ in Bingham fluids.

The simulation results are utilised to propose new correlations for $\overline{Nu}$ for both Newtonian and Bingham fluids guided by a scaling analysis. These correlations are shown to satisfactorily capture the variation of $\overline{Nu}$ with *Ra*, *Pr* and *Bn* for all the ranges of Rayleigh, Prandtl and Bingham numbers considered in this study.

## References


[1] S. Ostrach, Natural convection in enclosures, J. Heat Trans. 110 (1988) 1175–1190.
[2] J. Zhang, D. Vola, I.A. Frigaard, Yield stress effects on Rayleigh-Bénard convection, J. Fluid Mech. 566 (2006) 389–419.
[3] A. Vikhansky, Thermal convection of a viscoplastic liquid with high Rayleigh and Bingham numbers, Phys. Fluids 21 (2009) 103103.
[4] J. Pallsres, F.X. Grau, F. Giralt, Flow transitions in laminar Rayleigh-Bénard convection in cubical cavity at moderate Rayleigh numbers, Int. J. Heat Mass Trans. 42 (1999) 753–769.
[5] H.M. Park, D.H. Ryu, Rayleigh-Bénard convection of viscoelastic fluids in finite domains, J. Non-Newt. Fluid Mech. 98 (2001) 169–184.
[6] J. Pallsres, I. Cuesta, F.X. Grau, Laminar and turbulent Rayleigh-Bénard convection in a perfectly conducting cubical cavity, Int. J. Heat Fluid Flow 23 (2002) 346–358.
[7] H.M. Park, K.S. Park, Rayleigh-Bénard convection of viscoelastic fluids in arbitrary finite domains, Int. J. Heat Mass Trans. 47 (2004) 2251–2259.
[8] N. Quertatani, N.B. Cheikh, B.B. Beya, T. Lili, Numerical simulation of two dimensional Rayleigh-Bénard convection in an enclosure, C.R. Mecanique 336 (2008) 464–470.
[9] H. Ozoe, S.W. Churchill, Hydrodynamic stability and natural convection in Ostwald-De Waele and Ellis fluids: the development of a numerical solution, AIChE J. 18 (1972) 1196–1207.
[10] M. Lamsaadi, M. Naïmi, M. Hasnaoui, Natural convection of non-Newtonian power law fluids in a shallow horizontal rectangular cavity uniformly heated from below, Heat Mass Trans. 41 (2005) 239–249.
[11] N.J. Balmforth, A.C. Rust, Weakly nonlinear viscoplastic convection, J. Non-Newt. Fluid Mech. 158 (2009) 36–45.
[12] D. Vola, L. Boscardin, J.C. Latché, Laminar unsteady flows of Bingham fluids: a numerical strategy and some benchmark results, J. Computat. Phys. 187 (2003) 441–456.
[13] O. Turan, N. Chakraborty, R.J. Poole, Laminar natural convection of Bingham fluids in a square enclosure with differentially heated side walls, J. Non-Newt. Fluid Mech. 165 (2010) 901–913.
[14] O. Turan, R.J. Poole, N. Chakraborty, Aspect ratio effects in laminar natural convection of Bingham fluids in rectangular enclosures with differentially heated side walls, J. Non-Newt. Fluid Mech. 166 (2011) 208–230.
[15] O. Turan, A. Sachdeva, R.J. Poole, N. Chakraborty, Laminar natural convection of Bingham fluids in a square enclosure with vertical walls subjected to constant heat flux, Numer. Heat Trans. A 60 (2011) 381–409.
[16] H.A. Barnes, The yield stress—a review or παντα ρετ—everything flows?, J Non-Newt. Fluid Mech. 81 (1999) 133–178.
[17] E.J. O'Donovan, R.I. Tanner, Numerical study of the Bingham squeeze film problem, J. Non-Newt. Fluid Mech. 15 (1984) 75–83.
[18] T.C. Papanastasiou, Flow of materials with yield, J. Rheol. 31 (1987) 385–404.
[19] J. Peixinho, C. Desaubry, M. Lebouche, Heat transfer of a non-Newtonian fluid (Carbopol aqueous solution) in transitional pipe flow, Int. J. Heat Mass Trans. 51 (2008) 198–209.
[20] S.V. Patankar, Numerical Heat Transfer and Fluid Flow, Hemisphere, Washington, DC, 1980.
[21] P.J. Roache, Quantification of uncertainty in computational fluid dynamics, Annu. Rev. Fluid Mech. 29 (1997) 123–160.
[22] J. Cadafalch, C.D. Perez-Segarra, R. Còsul, A. Oliva, Verification of finite volume computations on steady-state fluid flow and heat transfer, ASME J. Fluids Eng. 124 (2002) 11–21.
[23] C. Ismail, O. Karatekin, Numerical experiments on application of Richardson extrapolation with nonuniform grids, ASME J. Fluids Eng. 119 (1997) 584–590.
[24] E. Mitsoulis, Flows of viscoplastic materials: models and computations, in: D.M. Binding, N.E. Hudson, R. Keunings (Eds.), Rheology Reviews, 2007, pp. 135–178.
[25] E. Mitsoulis, T. Zisis, Flow of Bingham plastics in a lid-driven square cavity, J. Non-Newt. Fluid Mech. 101 (2001) 173–180.
[26] A. Bejan, Convection Heat Transfer, John Wiley Sons Inc., New York, 1984.
[27] M. Corcione, Effects of the thermal boundary conditions at the sidewalls upon natural convection in rectangular enclosures heated from below and cooled from above, Int. J. Therm. Sci. 42 (2003) 199–208.